Molecular Blends of Methylated-Poly(ethylenimine) and Amorphous Porous Organic Cages for SO2 Adsorption

Journal:	*Journal of Materials Chemistry A*
Manuscript ID	TA-ART-03-2018-002788.R1
Article Type:	Paper
Date Submitted by the Author:	18-May-2018
Complete List of Authors:	Zhu, Guanghui; Georgia Institute of Technology, School of Chemical & Biomolecular Engineering Carrillo, Jan Michael; Oak Ridge National Laboarotry, Sujan, Achintya; Georgia Institute of Technology, School of Chemical & Biomolecular Engineering Okonkwo, Claudia; Georgia Institute of Technology, School of Chemical & Biomolecular Engineering Park, Sangjae; Georgia Institute of Technology, School of Chemical & Biomolecular Engineering Sumpter, Bobby; Oak Ridge National Laboratory, Computer Science and Mathematics Division and Center for Nanophase Materials Sci Jones, Christopher W.; Georgia Institute of Technology, School of Chemical & Biomolecular Engineering Lively, Ryan; Georgia Institute of Technology, School of Chemical & Biomolecular Engineering

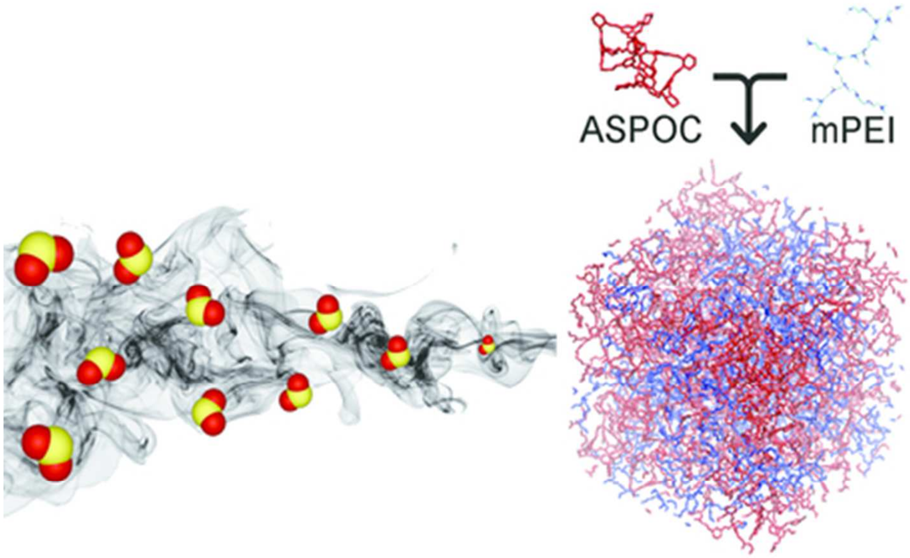

39x24mm (300 x 300 DPI)

Molecular Blends of Methylated-Poly(ethylenimine) and Amorphous Porous Organic Cages for SO_2 Adsorption

Guanghui Zhu[1,#], Jan-Michael Y. Carrillo[2,3,#], Achintya Sujan[1], Claudia N. Okonkwo[1], Sangjae Park[1], Bobby G. Sumpter[2,3,*], Christopher W. Jones[1,*], Ryan P. Lively[1,*]

1. School of Chemical & Biomolecular Engineering, Georgia Institute of Technology, Atlanta, Georgia 30332, United States

2. Center for Nanophase Materials Sciences, Oak Ridge National Laboratory, Oak Ridge, Tennessee 37831, United States

3. Computational Sciences and Engineering Division, Oak Ridge National Laboratory, Oak Ridge, Tennessee 37831, United States

Abstract: Porous organic cages (POCs) are emerging porous materials that exhibit intriguing properties in the areas of self-assembly, host-guest interaction, and solution processability. In this work, we explore the applicability of POCs as molecular porous supports for polymeric amines. We find that primary amines in poly(ethylenimine) (PEI) can undergo metathesis with the imine bonds present in POCs, resulting in non-porous products. This problem can be overcome by transforming the primary amines in PEI to tertiary amines via methylation. The methylated PEI (mPEI) forms homogeneous composites with amorphous scrambled porous organic cages (ASPOCs) without undesired reactions or phase separation. The microscopic structure of the composites is studied using molecular dynamics simulations. These composite materials are evaluated as adsorbents for low concentration SO_2 (200 ppm) adsorption and show good thermal and cyclic stability.

Introduction

Porous molecules such as porous organic cages (POCs) are emerging porous materials that have unique properties compared to traditional porous framework materials.[1-6] Due to their well-defined pores, tunability, solubility and processability, POCs have been explored in various applications related to molecular separations and gas storage.[7-14] In addition, POCs can be potentially used as a porous substrate for a wide range of functional materials including catalysts, adsorbents and drug delivery carriers.[15, 16] For example, it has been demonstrated that POCs can be used to immobilize rhodium nanoparticles, resulting in a "soluble" heterogeneous catalyst.[8]

POC molecules generally pack in the solid state as a crystalline phase as a result of weak van der Waals forces between adjacent POC molecules.[17] However, in some cases, such ordered packing can be disrupted. For example, in POCs made from trialdehydes and mixtures of diamine linkers the solid packing of the cage molecules is disrupted by the asymmetric cage exterior, which derives from the diamine mixture - such POCs are known as amorphous scrambled porous organic cages (ASPOCs).[18-20] Recently Jiang et al. reported the solution co-processing of functional materials with such organic cage molecules, whereby linear poly(ethylenimine) (PEI) was mixed with ASPOCs, and this mixing has shown positive synergistic effects on CO_2 uptake.[16]

The emission of acid gases such as CO_2, SO_x, and NO_x during fuel combustion poses environmental threats as well as health hazards.[21-26] Current industrial CO_2 removal and SO_2 scrubbing technologies suffer from high energy and material consumption, and can only be effectively applied to large stationary point sources.[27-31] Compared to absorption, adsorption using fixed-bed technologies has the benefit of low energy requirements, safety, and material consumption. Solid-supported amine materials have been recently proposed for various acid gas separations and studied extensively.[32, 33] Most of the solid supports investigated are inorganic porous materials such as mesoporous oxides and carbon-based materials.[34-42] Based on the earlier investigation by Jiang et al., in this work, we have explored the use of ASPOC materials as supports for acid gas adsorbing moieties, in particular, branched PEI. Branched PEI is commonly used in supported amine adsorbent studies because impregnation is straightforward, and in contrast to the long, straight chain of linear PEI, which mainly contains secondary amines, branched PEI possesses superior oxidation resistance and CO_2 capture performance due the presence of primary and tertiary amines, as well.[32, 43, 44] We initially impregnated branched PEI (~800 M_w) into ASPOC materials; however, ^1H NMR spectra of the resulting composite showed the loss of the characteristic shifts associated with PEI protons (Figure S1). This is attributed to a metathesis reaction between the primary amines at the chain ends in the branched PEI molecules and the imine bonds in the ASPOCs, forming new imine and enamine bonds. As a result, no PEI moieties were observed in the resulting composite (MALDI-MS in Figure S2). This cage-breaking reaction prevented the use of branched PEI in this type of composite.

To avoid the reaction between polyamines and ASPOCs, one can either change the chemistry of the cage to a platform that is more compatible with amines or alternatively, use tertiary amines that would not react with imine bonds. In this work, we adopted the second approach by converting primary and secondary amines in PEI to tertiary amines via methylation. Tertiary amines, including those on a PEI platform, have been previously explored as SO_2 sorbents supported in silica supports[45-47] where they were found to have favorable properties. In contrast, the adsorption of SO_2 on amine-supported solid materials containing primary and secondary amines typically leads to irreversible deactivation of the amines.[48-50] The reaction of SO_2 and tertiary amines forms reversible charge transfer complexes based on FTIR and ^{15}N NMR spectroscopic analysis,[45] but they adsorb little CO_2, which can be advantageous for the selective SO_2 capture from CO_2-containing streams.

Much like the solid supported PEI adsorbents reported in the literature, the reported tertiary amine adsorbents have been mostly limited to use of porous silica as a support.[45, 46] Importantly, the large pore size in many mesoporous silica materials can lead to the loss of active amine components due to evaporation.[46, 51] We hypothesized that the intimate mixing of porous organic cages with polymer molecules would result in good retention of the polymer during repeated thermal cycles, while still maintaining or even enhancing the performance of the adsorbing material. Here, we employ ASPOC supported methylated-PEI (mPEI) for SO_2 adsorption as an example to explore the limitations and potential of POC materials in energy and environmental applications. Our molecular dynamics simulations indicate an intimate mixing between mPEI and ASPOC molecules. We further experimentally evaluate the performance of the composite material for SO_2 adsorption.

Experimental

Materials. Triformylbenzene was purchased from Manchester Organics. Anhydrous dichloromethane, chloroform, ethylenediamine, (1R,2R)-1,2-cyclohexanediamine, branched PEI (800 M_w), were purchased from Sigma Aldrich. Ethyl acetate and diethyl ether was purchased from BDH Chemicals. Formic acid, 38% formaldehyde solution, potassium hydroxide pellets and magnesium sulfate were purchased from Alfa Aesar. Ultra-high purity N_2 and CO_2 gas cylinders were purchased from Airgas. Certified standard grade cylinders of 200 ppm SO_2 with a balancing of N_2 were purchased from Matheson Trigas. All chemicals were used as received without any purification.

Synthesis of ASPOC. The synthesis of the ASPOC $CC1_23_4$ (the subscripts denote the starting composition of the synthesis solution—2 equivalents of ethylenediamine (the linker for CC1) and 4 equivalents of (1R,2R)-1,2-cyclohexanediamine (the linker for CC3-R)) (Scheme 1) was carried out following a modified procedure from the literature.[18] To a solution of 500 mg triformylbenzene in 40 mL anhydrous dichloromethane (DCM), a solution of 90 mg ethylenediamine and 350 mg (1R,2R)-1,2-cyclohexanediamine in 40 mL anhydrous DCM was added. Then the mixture was stirred at room temperature for 3 days. A pale white powder was obtained by rotary evaporation. The product was washed with ethyl acetate to remove unreacted molecules and dried at 80 ºC under vacuum. Note that this synthesis will produce a mixture of cages that have different ethylenediamine and (1R,2R)-1,2-cyclohexanediamine distributions within each cage. The individual cages containing differing amounts of ethylenediamine and (1R,2R)-1,2-cyclohexanediamine are denoted as $CC1^x3^y$ in the simulation section, where x is the number of ethylenediamine molecules in a cage and y is the number of (1R,2R)-1,2-cyclohexanediamine molecules in the same cage.

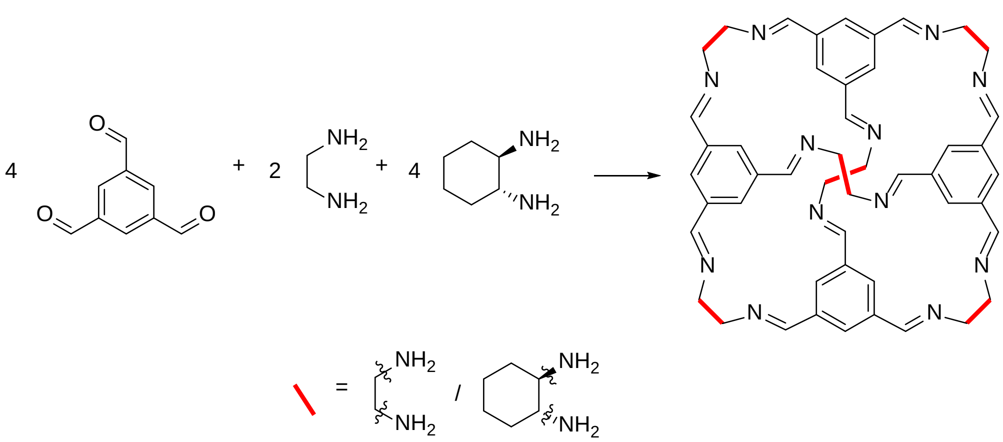

Scheme 1. Synthesis of ASPOC $CC1_23_4$ from 4 equivalents of triformylbenzene, 2 equivalents of ethylenediamine and 4 equivalents of (1R,2R)-1,2-cyclohexanediamine; which results in the formation of a mixture of cages.

Methylation of PEI. The N-methylation of PEI was carried out following a modified procedure from the literature.[45] Commercially available branched PEI (800 M_w, 1 g) was added to a round bottom flask equipped with a condenser containing 14 mL formic acid and 12 mL 38% formaldehyde solution. The flask was degassed on a Schlenk line and back-filled with N_2. The mixture was heated at 120 ºC overnight. The resultant solution was cooled to room temperature and transferred to an extraction funnel. Diethyl ether (50 mL) was added to the extraction funnel and KOH pellets were added to the flask until the organic layer turned yellow. The aqueous phase was washed one more time with diethyl ether and additional KOH pellets. The organic layer was dried over $MgSO_4$. The mPEI was obtained as a dark orange oil after rotary evaporation.

Preparation of mPEI/ASPOC composites. After drying, mPEI and ASPOC powder were dissolved in chloroform. Different mass ratios of mPEI to ASPOC were prepared as listed in Table S1 and denoted as 10-mPEI/ASPOC, 20-mPEI/ASPOC, and 40-

mPEI/ASPOC to represent the theoretical weight percent of mPEI in the final composite. The solvent was removed using rotary-evaporation. All samples showed no sign of phase separation and remained in powder form. A sample with 80 wt% mPEI loading was also prepared. However, this sample exhibited sticky surface characteristics and could not be handled as a free-flowing powder. 10-mPEI/ASPOC, 20-mPEI/ASPOC, and 40-mPEI/ASPOC samples were dried under dynamic vacuum at 60 °C to remove residual solvent. Elemental analysis was conducted to calculate the weight loading of mPEI.

SO_2 Adsorption Measurements. SO_2 adsorption, desorption and cyclic measurements in the composite materials were carried out using a gravimetric method employing a TA Instruments Q500 TGA with a modified furnace chamber. The feed flow rates of both the desorption and adsorption gases were fixed at 90 mL/min with the internal mass flow controller of the instrument and external mass flow controller for the N_2 pretreatment gas and sulfur-containing gas, respectively.

The activation temperature was determined with thermogravimetric analysis during the preparation of the mPEI/ASPOC composites. Adsorption of SO_2 was carried out at 25 °C and 35 °C with a cylinder of 200 ppm SO_2 balanced with N_2. Desorption of SO_2 was carried out in flowing N_2 at 60 °C and 90 °C based on the thermostability of the composites. Cyclic studies were carried out between 35 °C and 60 °C using the same time and flow conditions. Samples were cycled between high-temperature inert gas desorption and low-temperature SO_2 adsorption to determine cyclic stability.

Characterization methods

Electrospray Ionization – Mass Spectrometry (ESI-MS): ESI-MS of samples were taken on a Waters Quattro LC system.

Thermogravimetric analysis (TGA): the thermostability of polymer and composite materials was probed on a TA Instruments Q500 TGA. The samples were heated to desired temperature at 5 ºC/min under a flow of N_2 and held for 9 h.

NMR: Solution ^1H NMR spectra in $CDCl_3$ were recorded at 400.13 MHz using a Bruker Avance III 400 NMR spectrometer.

Scanning Electron Microscopy (SEM): high resolution imaging of the composite morphology was achieved using a Hitachi SU8230 Cold Field Emission Scanning Electron Microscope (CFE-SEM). The dry samples were attached to aluminum stubs using copper tape. The samples were then coated with a 20 nm layer of gold/palladium using a Hummer 6 Gold/Palladium Sputterer. Imaging was taken at a working distance of 8 mm and a working voltage of 3 kV using a mix of upper and lower secondary electron detectors.

Gas Sorption Analysis: porosity of the materials was assessed via nitrogen physisorption at 77 K using a Micromeritics ASAP2020HD. Surface areas were calculated from the data using the Brunauer–Emmett–Teller (BET) method. CO_2 isotherms were collected from the same equipment at 308 K.

Elemental analysis (EA) of CHN was performed by Atlantic Microlab.

Molecular Modeling. A simulation box, which was under periodic boundary conditions in the x, y and z directions, was randomly filled with n POC molecules having different types of vicinal diamines based on the composition for ASPOCs determined by Jiang et al.[18] (Scheme 2 (a)). Appropriate amounts of branched mPEI were added with the ASPOC such that the range of polymer loading was from 0 to 100 weight percent. The packing procedure is achieved with aid of PACKMOL.[52] Note that the branch architecture of PEI in Scheme 2 (b) and mPEI in Scheme 2 (c) is complementary, which means that the hydrogen atoms attached to primary (1^{o}) or secondary (2^{o}) amines in Scheme 2 (b) were replaced with methyl (-CH_3) groups in Scheme 2 (c), which would allow structural comparison between the methylated and unmethylated composites.

NPT ensemble atomistic molecular dynamics (AMD) simulations were performed using a Nosè-Hoover thermo- and barostat at 300 K and atmospheric pressure to equilibrate the simulation box. These simulations proceeded up to 40 ns, where the system density saturated and fluctuated to its equilibrium value. This was followed by a 10 ps simulation box deformation step to set the dimensions of the simulation box required to match that of the equilibrium density. Finally, a 1 ns NVT ensemble AMD simulation was used to collect the atom trajectories, stored every 5 ps, and subsequently used for characterizing the structure of the polymer/ASPOC composite.

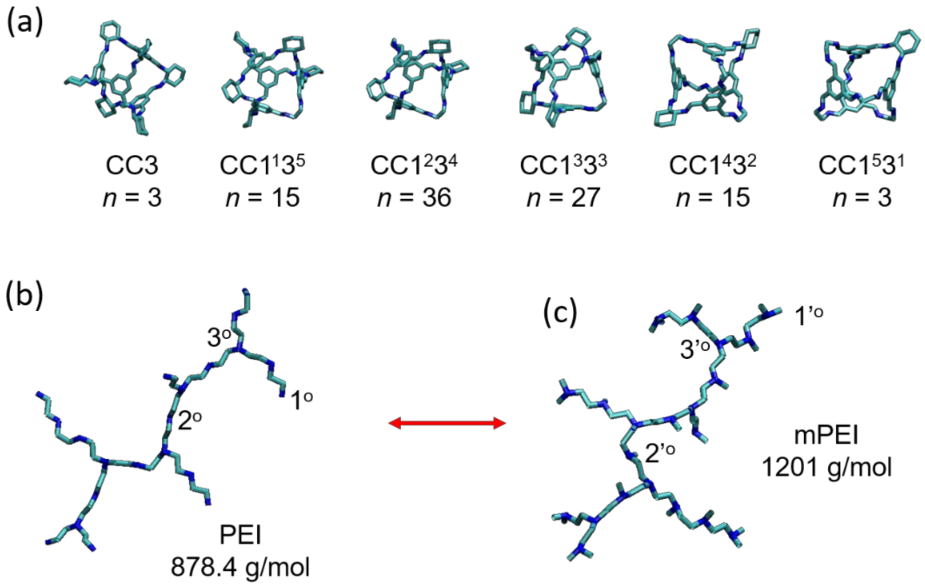

Scheme 2. (a) Composition of porous organic cages in the simulation box where $CC1^x3^y$ denotes a cage having x number of ethylenediamine and y number of diaminocyclohexane vicinal diamines, and *n* is the number of $CC1^x3^y$ molecules in the simulation box. (b) Structure of branched PEI with a molecular weight of 878.4 g/mol. C and N atoms are shown as cyan and blue cylinders, respectively, while H atoms are not shown. (c) Structure of mPEI with a molecular weight of 1201 g/mol and having the same branch architecture as in (b). The labels indicate the location of sample primary (1, 1'), secondary (2, 2') and tertiary (3, 3') amines in PEI and mPEI. The prime symbol indicates conversion of PEI to mPEI.

Results and Discussion

mPEI/ASPOC composites

We synthesized all tertiary amine containing PEI (mPEI) according to the procedure described in the experimental section.[45] The removal of all primary and secondary amines was confirmed by NMR and MS. Figure S3 shows the ^{1}H NMR spectra of PEI and mPEI. The amine protons (both primary and secondary) in PEI (1.75 ppm) entirely disappeared in the spectrum of mPEI and turned into a sharp peak at 2.23 ppm that was assigned to α-methyl protons, indicating methylation of all amine groups. Figure S4 shows the ESI-MS spectra of PEI and mPEI, as well as the theoretical molecular weight of the two polymers with increasing nitrogen units. A clear shift of the major peaks to a higher molecular weight corresponding to methylation can be observed.

The ASPOC sample was synthesized with an ethylenediamine to cyclohexanediamine linker ratio of 2:4. This ASPOC mixture has the least potential to crystallize among other cage mixtures (Figure S5). We hypothesize that this property will lead to molecular mixing with mPEI molecules instead of phase separation. The mPEI and ASPOC composite materials were prepared according to the procedure described in the experimental section. The three samples all appear as free-flowing powders. SEM images of the mPEI/ASPOC composite samples show random particle formation without noticeable aggregation (Figure S6). However, as the mPEI loading goes to 80 wt %, the particles became much bigger and showed signs of melting under the electron beam. The chemical compatibility between the mPEI and the ASPOC molecules was further checked with ^{1}H NMR and ESI-MS. In the ^{1}H NMR spectra (Figure S7) of mPEI/ASPOC composites, the proton signals from both the mPEI and ASPOC were retained in the composite materials. ESI-MS (Figure S8) spectra also suggest a physical mixture between mPEI and ASPOC molecules was obtained.

Structural characterization and molecular modeling of mPEI/ASPOC composites. The textural properties of the composite materials were initially characterized with N_2

physisorption at 77 K. However, in contrast to the gradual pore filling observed in most PEI/silica sorbent materials, the surface area and pore volume of the composite materials were virtually zero under the adsorption temperature of 77 K (Figure S9 (a)). This is because the mPEI molecules and ASPOC molecules likely form a “mixed matrix” composite rather than the typical, progressive pore filing observed in mesoporous supports,. At 77 K, the diffusion of N_2 gas into mPEI was extremely slow and thus could not reach the pores of the ASPOCs.

In contrast, CO_2 physisorption at elevated temperature (308 K) showed decreased uptake for the composite materials relative to the ASPOC materials (Figure S9b). Since tertiary amines in mPEI do not adsorb CO_2 under dry conditions, the CO_2 uptakes were also plotted normalized to ASPOC content in Figure S10. However, a decreasing trend was still present with increasing mPEI loading. This might be a result of mPEI molecules occupying the external or even internal pore volume of the ASPOC molecules. The external pore volume results from the random packing of the ASPOC molecules, which are responsible for part of the CO_2 uptake of the pure ASPOC. It is apparent that when mPEI molecules mix with ASPOC molecules, part of this volume will be occupied by mPEI. The internal pore volume is the volume held by the pores of the cages. It is unclear if this volume will be penetrated by mPEI molecule chain ends from the experimental results.

The microstructure of the composite materials was further studied using molecular dynamics simulations. The structural model of the composite materials with different mPEI loadings (which are slightly different than experimental values due to limitations of the simulation) were built as described in the methods section. Figure 1 shows the simulation box of the pure ASPOC as well as with around 40 wt% of mPEI molecules added to the box. As shown in the structure simulation of the 40-mPEI/ASPOC, the mPEI molecules are randomly distributed among ASPOC molecules without obvious agglomeration.

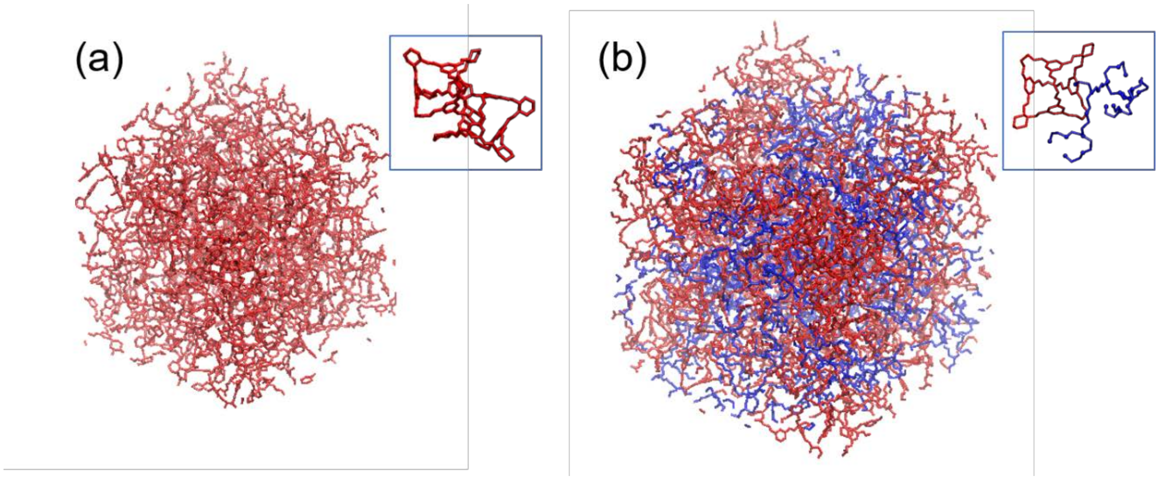

Figure 1. (a) Simulation box of ASPOC molecules according to the ratio shown in Scheme 2. (b) Simulation box of 40-mPEI/ASPOC.

The pore size distributions (PSDs) in the mPEI/ASPOC composites were estimated from the simulated structures. Here, we used the procedure by Bhattacharya and Gubbins with a probe particle of 1 Å diameter, in which the pore size is defined as the diameter of the largest sphere that encompasses a given point inside the pore that does not overlap with its neighboring wall atoms.[53] The average PSD as a function of polymer loading is shown in Figure 2, where the PSD was calculated from 20 configurations taken at a 50 ps interval from the NVT ensemble simulations. The bare ASPOC material has pore sizes ranging from 2 Å to 10 Å pore diameters with peaks located at 2 Å, 4 Å, and 5.5 Å. It can be further observed that as the mPEI loading is increased, the larger pores (4 Å and 5.5 Å) are being filled while small pores (2 Å) remained open.

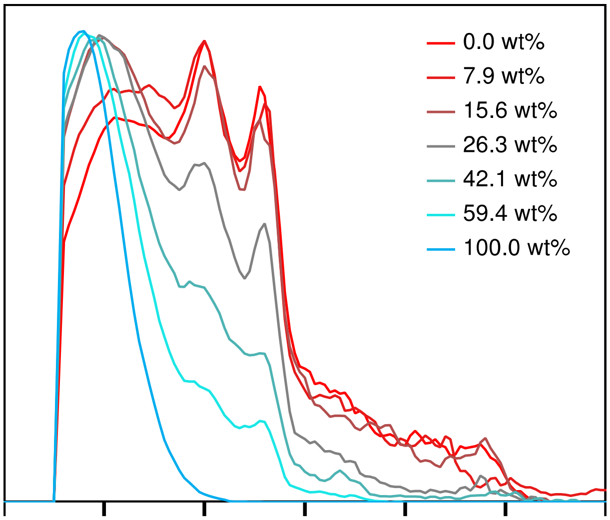

Figure 2. Pore size distribution (PSD) of mPEI and ASPOC composites as a function of mPEI loading.

The pair correlation or partial radial distribution functions *g(r)* presented in Figure 3 show the density probability for the center-of-mass of a POC to have a neighboring POC (top plot in Figure 3) or a polymer (bottom plot in Figure 3) at a given distance *r*. Note that the position vector of the center-of-mass is calculated with equal weights and does not discriminate between atoms, and *r* for each type of *g(r)* is illustrated in the images in Figure 3. No particular ordering can be noticed from the distribution functions, indicating a random mixing between the POC and mPEI molecules.

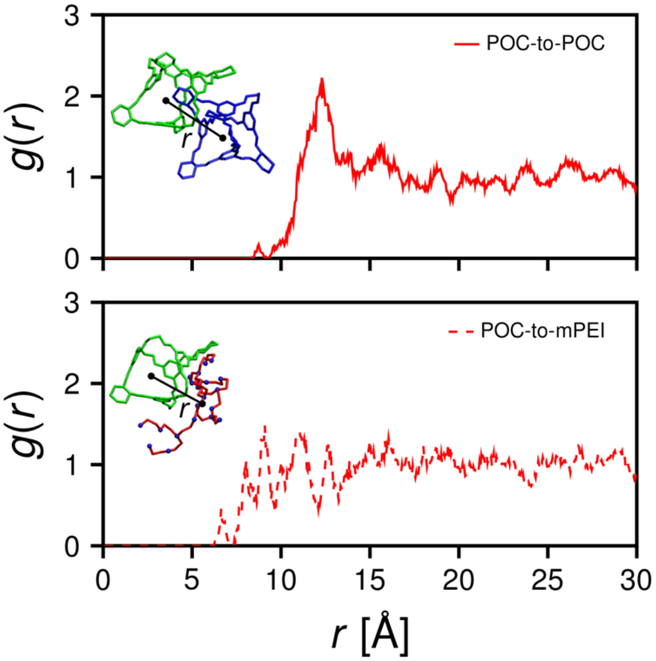

Figure 3. Partial radial distribution functions *g(r)* of the distance, *r*, which denotes the distance between the center-of-mass position between ASPOC molecules (top) and between 26.3% wt mPEI composites (bottom). The images in the inset depict the different definitions of *r*.

To explore whether the mPEI is filling the external pore volume or the internal pore volume, the *g(r)* analysis was expanded (Figure S11) to include the relative distances of the center-of-mass of POCs and between 1, 2, 3 (as well as methylated 1', 2', 3') amines. From Figure S11, we observed the following: (1) There is a higher probability for methylated 1' amines to be located nearer to the center of a POC in comparison to unmethylated 1 amines; (2) There is a lower probability for methylated 2' amines to be located nearer to the center of a POC in comparison to unmethylated 2 amines suggesting that 1' amines must have prevented 2' amines from occupying the center of the POC; (3) The *g(r)* for 3 amines and POCs in both methylated and unmethylated PEI remains relatively invariant, indicating that the branching topology is the main factor that determines the relative location of an amine from the center of a POC and not the amine type. This finding explains that the decreased CO_2 uptake in the composite materials is a result of both external and internal pore filling. While this type of microstructure may result in better mPEI retention, it may be detrimental to gas diffusion within the composite at high mPEI loadings.

The structure of the mPEI/ASPOC that can be summarized from the molecular simulations is: (1) mPEI molecules are dispersed among ASPOC molecules, the pores in the ASPOCs provide diffusion pathways for gas molecules to interact with tertiary amines in mPEI; (2) mPEI chain ends can penetrate the window of ASPOC molecules, such that at high loadings of mPEI, the pore network in the composite material is partially blocked and will significantly reduce the diffusion rate of gas molecules.

SO_2 adsorption measurements. The pseudo-equilibrium SO_2 capacities of the composite materials were determined gravimetrically with 200 ppm SO_2 in N_2 as the feed mixture. The capacities of the composite materials with different mPEI loadings were compared with pure ASPOC and mPEI as benchmarks. As shown in Figure 4 (a), the SO_2 capacities of each sample increased with mPEI loading. The final mPEI loadings were determined by elemental analysis and are listed in Table S1. Based on the tertiary amine amount calculated from the elemental analysis, the amine efficiency (mole SO_2 per mole amine) of each sample was estimated and is shown in Figure 4 (b). The amine efficiency of the composite samples decreased with increasing mPEI loading. This might be caused by steric hindrance, especially by amine moieties in the pores of ASPOC (predicted by molecular dynamics simulations) at the higher weight loading of mPEI in the ASPOC support.

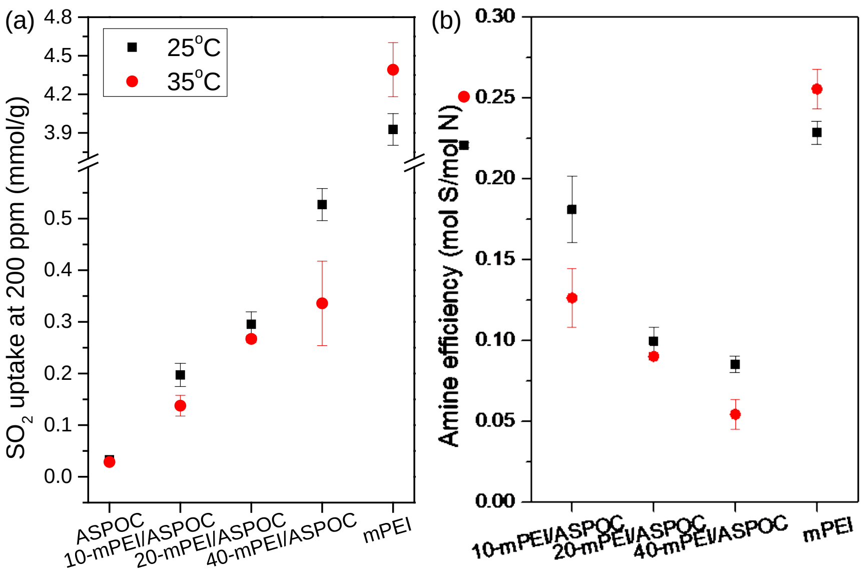

Figure 4. (a) SO_2 uptakes of pure ASPOC, mPEI and mPEI/ASPOC composites at 25ºC and 35 ºC; and (b) corresponding amine efficiencies. SO_2 uptake capacities for 40-mPEI/ASPOC are determined at 1000 min of adsorption as the uptake is slow and did not reach pseudo equilibrium.

The adsorption behavior of the mPEI/ASPOC composite at 35 °C was also studied. While pure ASPOC sample showed a minor difference with regards to the adsorption temperature, the composite samples showed a more pronounced decrease in SO_2 uptake. This is expected since the SO_2-tertiary amine interaction occurs exothermically with the formation of charge transfer complexes. A higher temperature will lead to a lower uptake capacity, which is ideal for regenerating the material after adsorption. On the other hand, the pure mPEI showed an opposite trend from the composite materials, with higher adsorption temperature leading to higher SO_2 uptake. This reversed temperature effect was also observed in PEI/silica adsorbents for CO_2.[34, 54, 55] It was elucidated by neutron diffraction studies that the PEI molecules in mesoporous SBA-15 silica supports form liquid phase films or plugs in the pores.[56] A higher adsorption temperature will improve the flexibility of the polymer chains and allow for the system to approach closer to thermodynamic equilibrium. However, the higher temperature leads to a decrease in the thermodynamic equilibrium capacity, which is undesirable. From our molecular dynamics simulations, the mPEI and ASPOC molecules will form a molecular scale mixture instead of separated phases, thus changing the inverse temperature effect observed in the case of PEI/silica adsorbents.

Although the 10-mPEI/ASPOC displayed a much lower SO_2 uptake compared to the pure mPEI at both temperatures, the amine efficiency was only slightly lower, indicating that the performance was maintained in terms of amine utility in the composite materials at low mPEI loadings. More importantly, the uptake kinetics in the composite materials (Figure 5) showed an improvement of the SO_2 uptake rate in the composite material. While this holds true for 10-mPEI/ASPOC and 20-mPEI/ASPOC samples, the 40-mPEI/ASPOC material showed a much slower uptake rate compared to the other samples. This is likely because of the impeded gas diffusion from the high degree of chain-end penetration into the ASPOC pores, as predicted in the molecular simulations. It can be observed that in this particular experiment mPEI reaches saturation at a time close to that for 10-mPEI/ASPOC and 20-mPEI/ASPOC. This is a result of the small amount of mPEI sample utilized in the experiment to measure the saturation within reasonable time duration. If more mPEI is used in the analysis, the time at which mPEI and composite materials reaches equilibrium will be different.

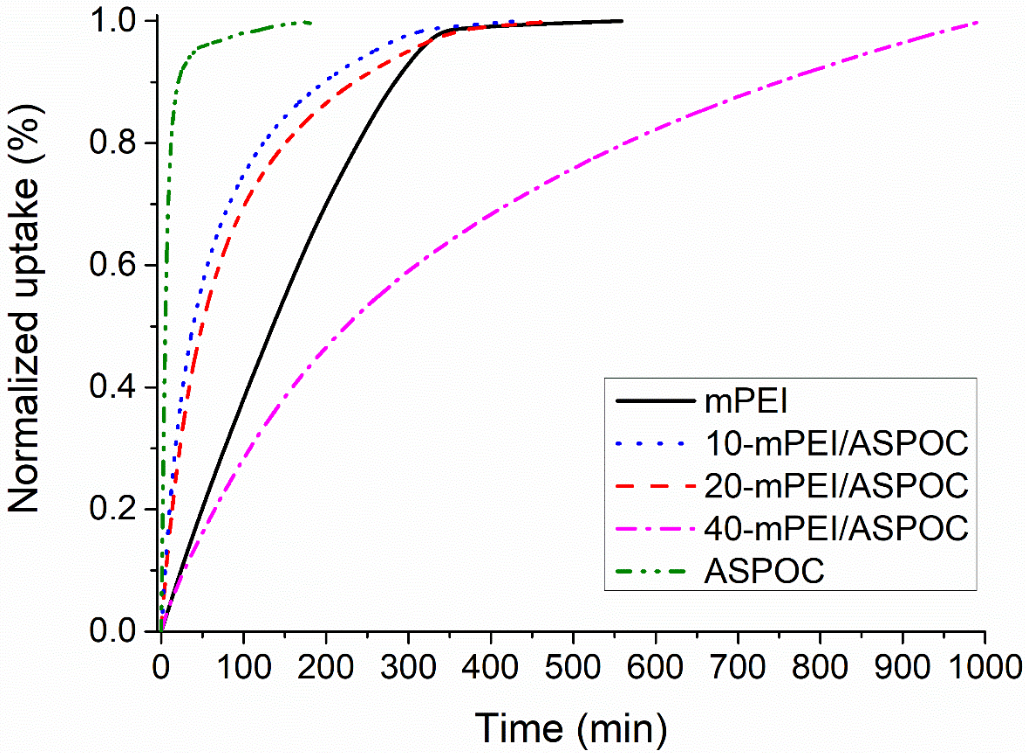

Figure 5. SO_2 adsorption kinetics in pure mPEI, ASPOC and mPEI/ASPOC composites at 25ºC

Thermostability and Regeneration of Adsorbents. Since the methylation of primary and secondary amines will reduce the number and strength of hydrogen-bond interactions between polymer molecules, the mPEI species are expected to be more volatile than PEI. Figure 6 (a) shows the relative volatility of mPEI compared to PEI at 3 different temperatures relevant to desorption conditions. It was observed that the mPEI exhibits a higher volatility at all temperatures tested, which might undermine the reusability of the composite material under cyclic operation. With this in mind, we investigated the thermostability of the composite materials. Figure S13 shows the normalized weight loss of the three composite samples being held at different temperatures (60 °C, 90 °C, and 120 °C). The initial weight loss is attributed to desorption of moisture, as evidenced by online mass spectrometry analysis of the desorbed species. (Figure S14 and S15) When compared across different samples, a higher mPEI loading resulted in a larger initial weight loss, which is attributed to more adsorbed moisture.

The rates of weight loss are calculated from the slopes shown in Figure 6 (a) (detailed fitting parameters can be found in Figure S12 and S13) and shown in Figure 6 (b). The incorporation of mPEI into the ASPOC greatly increased its retention during high temperature exposure as a result of the formation of a solid solution and entanglement of the mPEI with the ASPOC pore structure. It was observed that the composite material was stable to at least 90 °C exposure. At 120 °C, a gradual loss in weight was observed due to slow evaporation of mPEI in the material.

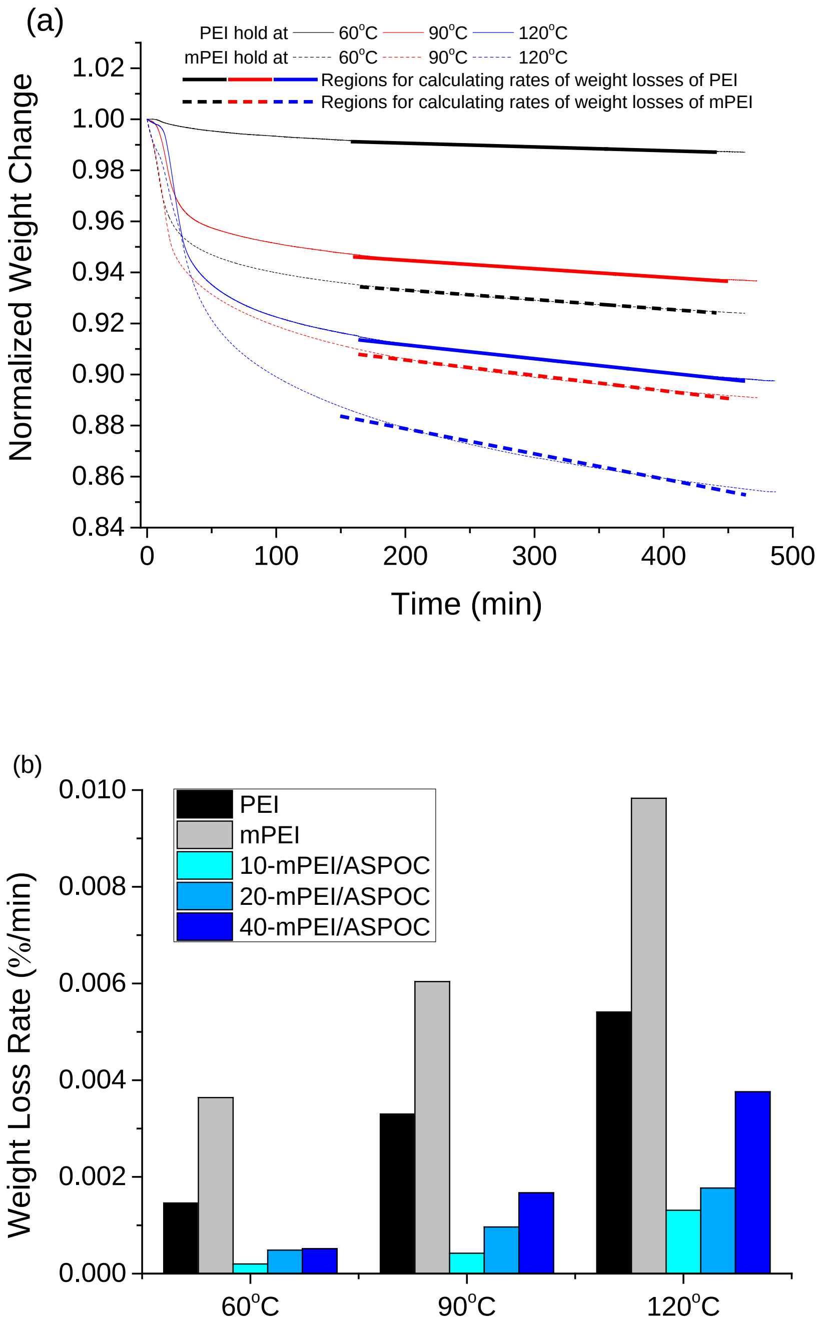

Figure 6. (a) Thermal stability of the PEI and mPEI at 60 °C, 90 °C, and 120 °C, and corresponding regions for calculating rates of weight losses. (b) rate of weight loss of the composite samples, PEI and mPEI under 60 °C, 90 °C, and 120 °C.

The regeneration of the composite, i.e., desorption of the adsorbed SO_2, was also studied at the three temperatures used above. A fresh sample was used at each temperature. The sample was first activated at either 60 °C, 90 °C, or 120 °C, followed by adsorption of SO_2 at 25 °C for 360 min, and thermal desorption at the same activation temperature. The SO_2 uptake capacities were then compared between each sample. In addition, the regenerability was evaluated by comparing the final sample weight to the activated sample weight. Figure 7 shows the weight change of the 20-mPEI/ASPOC sample under different activation/desorption temperatures. At the desorption temperature of 60 °C, the adsorbed SO_2 did not fully desorb. However, at 90 °C and 120 °C, the weights after desorption were lower than the starting weight, indicating a further loss of polymer and/or moisture from the adsorbents.

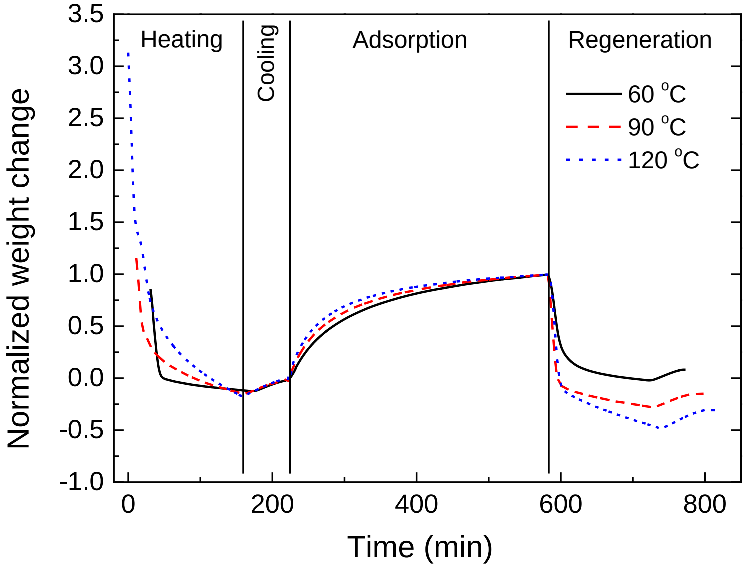

Figure 7. Weight change profiles of 20-mPEI/ASPOC during activation-adsorption-regeneration cycle under 60 °C, 90 °C, and 120 °C. The data are normalized by sample dry weight.

Cyclic Adsorption Study. The results from the thermostability and regeneration studies indicate the potential of the mPEI/ASPOC composite materials to be used as stable SO_2 sorbents with a small swing temperature between 25 °C and 60 °C. Thus, the cyclic stability of 20-mPEI/ASPOC was studied in a temperature swing adsorption cycle with adsorption at 25 °C and desorption at 60 °C. The cyclic capacities are shown in Figure 8. It can be observed that, except the drop in the first cycle, the sample appeared stable after approximately 8 cycles. The amine efficiency of the sample during the 12 total cycles is plotted in Figure S17. The capacity drop in the first cycle is probably due to some SO_2 molecules not fully desorbing from the strongest base sites at this low regeneration temperature.

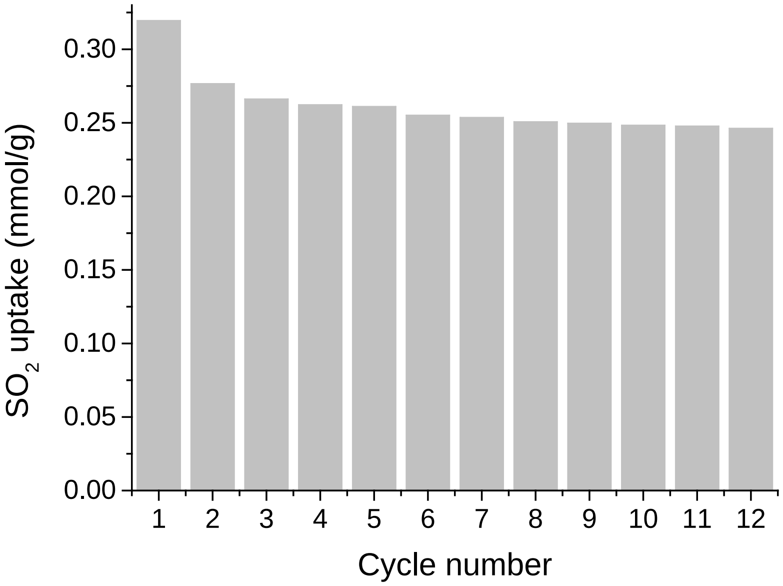

Figure 8. Cyclic SO_2 uptake performance of 20-mPEI/ASPOC with a sorption temperature of 25°C and a desorption temperature of 60°C.

Conclusions

In this work, we explored the applicability of imine-based POCs as a potential support for SO_2-sorbing polymers. The imine based POCs were found to react with primary and secondary amines in branched poly(ethylenediamine). We then prepared a series of composites with a fully tertiary poly(amine) sample utilizing mPEI as the sorbing phase and ASPOCs as the support/substrate. It was observed that the mPEI molecules can form a solid solution with the ASPOC molecules. The hypothesized structure was supported by molecular dynamics simulations. The thermostability and SO_2 capacity of the composite materials were studied as a function of the mPEI loading. The composite materials were found to have improved uptake kinetics and comparable amine efficiencies with the pure mPEI. A representative sample was tested in a simulated temperature swing adsorption-desorption cycle and showed stable cyclic performance at low SO_2 concentration.

Compared to oxide and carbon substrates, POCs can suffer from higher cost and instability. We have shown that more cost-effective feed stocks can be used to reduce the cost of POCs and at the same time, increase their acid gas stability.[57] In this work, we only considered impregnated amines. Compared to grafted amines, impregnated amines are less thermally stable but have the advantages of easy preparation and high amine loading.[58] By introducing surface functional groups, grafted amines can also conceptually be applied to POC materials.[59] When choosing POCs as porous substrates, the following points have to be taken into consideration. (1) Compatibility between the POC molecules and the active adsorbent molecule. (2) Stability of POC molecules under the desired operating conditions. For example, in drug delivery applications, the reversibility (instability) of the cage-forming bonds is required. On the other hand, in many catalysis or separation applications, the POCs are expected to be stable. (3) There should be a potential benefit of creating composite materials compared to bare components.

Conflicts of interest

There are no conflicts to declare.

Acknowledgments

This work was supported by the Center for Understanding and Control of Acid Gas-Induced Evolution of Materials for Energy (UNCAGE-ME), an Energy Frontier Research Center funded by U.S. Department of Energy (US DoE), Office of Science, Basic Energy Sciences (BES), under Award DE-SC0012577. This work was performed in part at the Georgia Tech Institute for Electronics and Nanotechnology, a member of the National Nanotechnology Coordinated Infrastructure, which is supported by the National Science Foundation (Grant ECCS-1542174). Computational aspects of this work were performed at the Center for Nanophase Materials Sciences (CNMS), which is a US DOE Office of Science User Facility. Some of the research used resources of the Oak Ridge Leadership Computing Facility (OLCF) at the Oak Ridge National Laboratory (ORNL), which is supported by the Office of Science of the U.S. DOE under Contract DE-AC05-00OR22725.

Notes and references

Corresponding Authors

*E-mail: sumpterbg@ornl.gov (B.G.S)

*E-mail: christopher.jones@chbe.gatech.edu (C.W.J)

*E-mail: ryan.lively@chbe.gatech.edu (R.P.L)

Author Contributions

[#] G.Z. and J.Y.C. contributed equally to this work.

1. A. G. Slater, M. A. Little, M. E. Briggs, K. E. Jelfs and A. I. Cooper, *Mol. Syst. Des. Eng.*, 2018, **3**, 223-227.
2. S. Jiang, Q. Song, A. Massey, S. Y. Chong, L. Chen, S. Sun, T. Hasell, R. Raval, E. Sivaniah, A. K. Cheetham and A. I. Cooper, *Angew. Chem. Int. Ed.*, 2017, **56**, 9391-9395.
3. S. Tothadi, M. A. Little, T. Hasell, M. E. Briggs, S. Y. Chong, M. Liu and A. I. Cooper, *CrystEngComm*, 2017, **19**, 4933-4941.
4. J. T. A. Jones, D. Holden, T. Mitra, T. Hasell, D. J. Adams, K. E. Jelfs, A. Trewin, D. J. Willock, G. M. Day, J. Bacsa, A. Steiner and A. I. Cooper, *Angew. Chem. Int. Ed.*, 2011, **50**, 749-753.
5. M. A. Little, S. Y. Chong, M. Schmidtmann, T. Hasell and A. I. Cooper, *Chem. Commun.*, 2014, **50**, 9465-9468.
6. T. Hasell, M. Miklitz, A. Stephenson, M. A. Little, S. Y. Chong, R. Clowes, L. J. Chen, D. Holden, G. A. Tribello, K. E. Jelfs and A. I. Cooper, *J. Am. Chem. Soc.*, 2016, **138**, 1653-1659.
7. X. Zou and G. Zhu, *Adv. Mater.*, 2018, **30**, 1700750.
8. J. K. Sun, W. W. Zhan, T. Akita and Q. Xu, *J. Am. Chem. Soc.*, 2015, **137**, 7063-7066.
9. Q. L. Song, S. Jiang, T. Hasell, M. Liu, S. J. Sun, A. K. Cheetham, E. Sivaniah and A. I. Cooper, *Adv. Mater.*, 2016, **28**, 2629-2637.
10. T. Uemura, R. Nakanishi, S. Mochizuki, S. Kitagawa and M. Mizuno, *Angew. Chem. Int. Ed.*, 2016, **55**, 6443-6447.
11. S. M. Xie, J. H. Zhang, N. Fu, B. J. Wang, L. Chen and L. M. Yuan, *Anal. Chim. Acta*, 2016, **903**, 156-163.
12. M. A. Zwijnenburg, E. Berardo, W. J. Peveler and K. E. Jelfs, *J. Phys. Chem. B*, 2016, **120**, 5063-5072.
13. J. Dechnik, J. Gascon, C. J. Doonan, C. Janiak and C. J. Sumby, *Angew. Chem. Int. Ed.*, 2017, **56**, 9292-9310.

14. M. Ortiz, S. Cho, J. Niklas, S. Kim, O. G. Poluektov, W. Zhang, G. Rumbles and J. Park, *J. Am. Chem. Soc.*, 2017, **139**, 4286-4289.
15. D. Zhao, S. Tan, D. Yuan, W. Lu, Y. H. Rezenom, H. Jiang, L.-Q. Wang and H.-C. Zhou, *Adv. Mater.*, 2011, **23**, 90-93.
16. S. Jiang, L. Chen, M. E. Briggs, T. Hasell and A. I. Cooper, *Chem. Commun.*, 2016, **52**, 6895-6898.
17. M. J. Bojdys, M. E. Briggs, J. T. A. Jones, D. J. Adams, S. Y. Chong, M. Schmidtmann and A. I. Cooper, *J. Am. Chem. Soc.*, 2011, **133**, 16566-16571.
18. S. Jiang, J. T. A. Jones, T. Hasell, C. E. Blythe, D. J. Adams, A. Trewin and A. I. Cooper, *Nat. Commun.*, 2011, **2**, 207.
19. N. Giri, C. E. Davidson, G. Melaugh, M. G. Del Popolo, J. T. A. Jones, T. Hasell, A. I. Cooper, P. N. Horton, M. B. Hursthouse and S. L. James, *Chem. Sci.*, 2012, **3**, 2153-2157.
20. N. Giri, M. G. Del Popolo, G. Melaugh, R. L. Greenaway, K. Ratzke, T. Koschine, L. Pison, M. F. C. Gomes, A. I. Cooper and S. L. James, *Nature*, 2015, **527**, 216-220.
21. J. T. Houghton, Y. Ding, D. J. Griggs, M. Noguer, P. J. van der Linden, X. Dai, K. Maskell and C. A. Johnson, *Climate change 2001: the scientific basis*, The Press Syndicate of the University of Cambridge, 2001.
22. M. Z. Jacobson, *Energy Environ. Sci.*, 2009, **2**, 148-173.
23. *World health statistics 2017: monitoring health for the SDGs, Sustainable Development Goals*, World Health Organization, 2017.
24. J. H. Seinfeld and S. N. Pandis, *Atmospheric chemistry and physics: from air pollution to climate change*, John Wiley & Sons, 2016.
25. E. Barea, C. Montoro and J. A. R. Navarro, *Chem. Soc. Rev.*, 2014, **43**, 5419-5430.
26. M. Kampa and E. Castanas, *Environ. Pollut.*, 2008, **151**, 362-367.
27. P. V. Danckwerts, *Chem. Eng. Sci.*, 1979, **34**, 443-446.
28. D. Y. C. Leung, G. Caramanna and M. M. Maroto-Valer, *Renewable Sustainable Energy Rev.*, 2014, **39**, 426-443.
29. J. T. Yeh, K. P. Resnik, K. Rygle and H. W. Pennline, *Fuel Process. Technol.*, 2005, **86**, 1533-1546.
30. S.-H. Jung, G.-T. Jeong, G.-Y. Lee, J.-M. Cha and D.-H. Park, *Korean J. Chem. Eng.*, 2007, **24**, 1064-1069.
31. S. Ebrahimi, C. Picioreanu, R. Kleerebezem, J. J. Heijnen and M. C. M. van Loosdrecht, *Chem. Eng. Sci.*, 2003, **58**, 3589-3600.
32. S. Choi, J. H. Drese and C. W. Jones, *ChemSusChem*, 2009, **2**, 796-854.
33. S.-Y. Lee and S.-J. Park, *J. Ind. Eng. Chem.*, 2015, **23**, 1-11.
34. X. Xu, C. Song, J. M. Andresen, B. G. Miller and A. W. Scaroni, *Energy & Fuels*, 2002, **16**, 1463-1469.
35. X. Xu, C. Song, B. G. Miller and A. W. Scaroni, *Ind. Eng. Chem. Res.*, 2005, **44**, 8113-8119.
36. X. Xu, C. Song, J. M. Andrésen, B. G. Miller and A. W. Scaroni, *Microporous Mesoporous Mater.*, 2003, **62**, 29-45.

37. X. Xu, C. Song, B. G. Miller and A. W. Scaroni, *Fuel Process. Technol.*, 2005, **86**, 1457-1472.
38. K. Huang, S.-H. Chai, R. T. Mayes, G. M. Veith, K. L. Browning, M. A. Sakwa-Novak, M. E. Potter, C. W. Jones, Y.-T. Wu and S. Dai, *Chem. Commun.*, 2015, **51**, 17261-17264.
39. M. E. Potter, K. M. Cho, J. J. Lee and C. W. Jones, *ChemSusChem*, 2017, **10**, 2192-2201.
40. S. H. Pang, L.-C. Lee, M. A. Sakwa-Novak, R. P. Lively and C. W. Jones, *J. Am. Chem. Soc.*, 2017, **139**, 3627-3630.
41. M. G. Plaza, C. Pevida, A. Arenillas, F. Rubiera and J. J. Pis, *Fuel*, 2007, **86**, 2204-2212.
42. E. P. Dillon, C. A. Crouse and A. R. Barron, *ACS Nano*, 2008, **2**, 156-164.
43. A. Heydari-Gorji, Y. Belmabkhout and A. Sayari, *Microporous Mesoporous Mater.*, 2011, **145**, 146-149.
44. P. Bollini, S. Choi, J. H. Drese and C. W. Jones, *Energy Fuels*, 2011, **25**, 2416-2425.
45. R. Tailor, M. Abboud and A. Sayari, *Environ. Sci. Technol.*, 2014, **48**, 2025-2034.
46. R. Tailor, A. Ahmadalinezhad and A. Sayari, *Chem. Eng. J.*, 2014, **240**, 462-468.
47. R. Tailor and A. Sayari, *Chem. Eng. J.*, 2016, **289**, 142-149.
48. A. P. Hallenbeck and J. R. Kitchin, *Ind. Eng. Chem. Res.*, 2013, **52**, 10788-10794.
49. A. Diaf, J. L. Garcia and E. J. Beckman, *J. Appl. Polym. Sci.*, 1994, **53**, 857-875.
50. P. Bollini, S. A. Didas and C. W. Jones, *J. Mater. Chem.*, 2011, **21**, 15100-15120.
51. Y. Zhi, Y. Zhou, W. Su, Y. Sun and L. Zhou, *Ind. Eng. Chem. Res.*, 2011, **50**, 8698-8702.
52. L. Martínez, R. Andrade, E. G. Birgin and J. M. Martínez, *J. Comput. Chem.*, 2009, **30**, 2157-2164.
53. S. Bhattacharya and K. E. Gubbins, *Langmuir*, 2006, **22**, 7726-7731.
54. M. B. Yue, Y. Chun, Y. Cao, X. Dong and J. H. Zhu, *Adv. Funct. Mater.*, 2006, **16**, 1717-1722.
55. W.-J. Son, J.-S. Choi and W.-S. Ahn, *Microporous Mesoporous Mater.*, 2008, **113**, 31-40.
56. A. Holewinski, M. A. Sakwa-Novak and C. W. Jones, *J. Am. Chem. Soc.*, 2015, **137**, 11749-11759.
57. Z. Guanghui, H. C. D., L. Yang, B. Souryadeep, T. Uma, J. M. L., W. Zili, S. D. S., N. Sankar, J. C. W. and L. R. P., *Chem. - Eur. J.*, 2016, **22**, 10743-10747.
58. S. A. Didas, S. Choi, W. Chaikittisilp and C. W. Jones, *Acc. Chem. Res.*, 2015, **48**, 2680-2687.
59. G. Zhu, Y. Liu, L. Flores, Z. R. Lee, C. W. Jones, D. A. Dixon, D. S. Sholl and R. P. Lively, *Chem. Mater.*, 2018, **30**, 262-272.